AGN effect on cooling flow dynamics

F. Alouani Bibi, J. Binney, K. Blundell and H. Omma

arXiv:0706.2949v2 [astro-ph] 11 Jul 2007

Abstract We analyzed the feedback of AGN jets on cooling flow clusters using three-dimensional AMR hydrodynamic simulations. We studied the interaction of the jet with the intracluster medium and creation of low X-ray emission cavities (Bubbles) in cluster plasma. The distribution of energy input by the jet into the system was quantified in its different forms, i.e. internal, kinetic and potential. We find that the energy associated with the bubbles, $(pV + \gamma pV/(\gamma - 1))$, accounts for less than 10 percent of the jet energy.

Keywords Cooling flow, galaxy cluster, AGN jet, bubble, feedback: general

1 Introduction

During the last two decades clusters with cooling flows have been extensively studied. Prior to results obtained by XMM-Newton and Chandra it was widely believed that in these systems up to $1000 M_\odot \, \mathrm{yr}^{-1}$ of gas was moving from the hot phase $T > 10^7 \, \mathrm{K}$ to low temperatures. In this picture extensive emission by Fe XVII ions was predicted, in contradiction with spectra obtained by XMM-Newton (Peterson et al. 2003). The reasons for this conflict between theory and observation are discussed in papers by Omma et .al (2004), Binney (2005) and Pizzalato & Soker (2005).

It is now widely accepted that feedback from AGN jets is responsible for slowing or halting the cooling of gas in galaxy groups and clusters (Churazov et al. 2000; Birzan et al. 2004; Binney et al. 2007), and it is likely that this phenomenon also takes place in elliptical galaxies at smaller (spatial and temporal) scales (Binney & Tabor 1995).

F. Alouani Bibi, J. Binney, K. Blundell and H. Omma

St Johns Research Centre University of Oxford, Oxford OX1 3JP, UK

AGN jets reheat hot gas by doing mechanical work during the inflation of low-density bubbles. The Chandra observatory has now detected bubbles as regions of low X-ray emission in a large number of systems (Carilli et al. 1994; David et al. 2001; McNamara et al. 2000; Fabian et al. 2001). Most, but not all bubbles are associated with non-thermal radio emission (Birzan et al. 2004), and when both radio-loud and radio-quiet bubbles occur, the radio-quiet bubbles are further from the center. Thus it appears that bubbles are radio-loud for a period after inflation, and a combination of adiabatic expansion of the plasma and radiative losses by the most energetic electrons makes the bubble radio-quiet.

In some cases a synchrotron-emitting jet runs from the galactic nucleus to the bubbles, so jets are definitely involved in bubble formation. It is unclear to what extent bubbles are driven by the relativistic cores of the jets rather than the slower and more massive flows that probably surround the cores. We are also uncertain whether the jets are driven by the black hole's accretion disk or emerge from its ergosphere (Blandford & Znajek 1977), but the observation of fast jets in microquasars that are known to be powered by neutron stars suggests that an ergosphere does not need to be involved (Nipoti et al. 2005).

2 Method

To investigate how an AGN jet interacts with cluster gas, we performed a series of three-dimensional hydrodynamic simulations using the code Enzo (Bryan & Norman 1997). Because of the inhomogeneity of the plasma, we used the adaptive grid refinement (AMR) technique to subdivide the simulation domain, which was a cube $L = 614 \, \mathrm{kpc}$ on a side. Our coarsest grid

has 16 cells in each direction, and in the lth level of refinement the effective number of grid points is increased to 16×2^l, where $l = 0, \ldots, 6$. The cluster core is at the 6th refinement level, so the grid would have 1024^3 cells if the entire domain were refined to this level. We used the piecewise parabolic method PPM (Woodward & Collela 1984) Riemann solver to advance the hydrodynamic equations.

In previous simulations the effects of jets have been taken into account by one of three techniques: (i) an inner boundary is introduced on which inflow boundary conditions can be set (Basson & Alexander 2003); (ii) spherical cavities are carved out of the ambient medium and filled with much less dense material that provides a similar pressure (Churazov et al. 2001); (iii) at some arbitrarily chosen locations, energy is added at some specified rate (Brüggen & Kaiser 2002). Our technique differs from approach (iii) in that we add mass, momentum and energy on two small, centrally located "injection disks" of radius $r_{\text{jet}} = 3\,\text{kpc}$ (Omma et al. 2004). The ratio of the rates of injection of mass, $\dot{m}_{\text{jet}} = 1 M_\odot\,\text{yr}^{-1}$, and momentum specify the jet speed $v_{\text{jet}} = 4 \times 10^4\,\text{km}\,\text{s}^{-1}$, which is sub-relativistic but supersonic. As the simulation develops, the region in which the injected energy is largely thermalized moves away from the center, just as the hot spot of a real system should. Hence we believe our technique is more realistic than either technique (ii) or technique (iii), and it avoids the introduction of the unphysical inner boundary required by technique (i). We implement this scheme by solving the equations

$$\frac{\partial \rho}{\partial t} + \overrightarrow{\nabla} \cdot \rho\,\overrightarrow{v} = \chi \dot{m}_{\text{jet}} \tag{1}$$

$$\frac{\partial \rho\,\overrightarrow{v}}{\partial t} + \overrightarrow{\nabla} \cdot (\rho\,\overrightarrow{v} \otimes \overrightarrow{v}) = -\overrightarrow{\nabla}p - \rho\overrightarrow{\nabla}\Phi + \chi \dot{m}_{\text{jet}} v_{\text{jet}}\,\overrightarrow{i} \tag{2}$$

$$\frac{\partial E}{\partial t} + \overrightarrow{\nabla} \cdot (E\,\overrightarrow{v}) = -\overrightarrow{\nabla} \cdot p\,\overrightarrow{v} - \rho\,\overrightarrow{v} \cdot \overrightarrow{\nabla}\Phi + \chi E_{\text{jet}} - j_{\text{rad}} \tag{3}$$

where ρ, v, p, and E are the mass density, velocity, thermal pressure and total energy, respectively, Φ is the gravitational potential, $E_{\text{jet}} = \frac{1}{2}\dot{m}v_{\text{jet}}^2$, j_{rad} is rate per unit volume of radiative energy loss, and χ is a window function that vanishes outside the injection disk. On the disk

$$\chi(r) = \begin{cases} e^{-3r^2/2r_{\text{jet}}^2} & r \le r_{\text{jet}} \\ 0 & r > r_{\text{jet}}, \end{cases} \tag{4}$$

where r is distance from the jet axis. The cluster baryonic matter is assumed to evolve in a dark-matter halo,

described by the NFW model (Navarro et al. 1995). The mass within a sphere of radius r is

$$M(r) = 4\pi\delta_c\rho_c r_s^3 \left[\ln(1 + r/r_s) - \frac{r/r_s}{1 + r/r_s}\right], \tag{5}$$

where ρ_c is the critical density of the universe at the cluster redshift, r_s is the scale radius of the cluster and δ_c is the overdensity parameter (David et al. 2001)

$$\rho_c = \frac{3H^2}{8\pi G} \tag{6}$$

$$\delta_c = \frac{200}{3}\frac{(r_{200}/r_s)^3}{\ln(1 + r_{200}/r_s) - \frac{r_{200}/r_s}{1+r_{200}/r_s}}, \tag{7}$$

where r_{200} is the radius within which the average density is equal to $200\rho_c$. In our simulations δ_c and r_s were equal to 7.48×10^4 and $77\,\text{kpc}$, respectively. The initial electron density was

$$n_e(r) = 0.1 \left(1 + \frac{r}{50\,\text{kpc}}\right)^{-2.7}\,\text{cm}^{-3}. \tag{8}$$

This provides a good fit to the Hydra cluster density profile reported by David et al. (2001). As initial condition we assume that the system is in hydrostatic equilibrium and deduce the initial temperature profile from the assumption that the plasma is an ideal gas.

To have a self-consistent model for jet power, one should assume that an AGN's outbursts are conditioned by the accretion rate of the black hole lurking at the center of the cluster. The accretion rate will depend on the rate of inflow of matter toward the cluster core due to radiative cooling loses, which form a self-sustained loop (Binney & Tabor 1995; Cattaneo & Teyssier 2007). Here we assumed fixed power and duration of the jet based on observational estimates of known AGN jets (Table 1).

3 Results

The cluster is allowed to cool passively for 3×10^8 yr using line and continuum radiation (Sutherland & Dopita 1993). The cooling function Λ is represented in (Fig. 1) as a function of the gas temperature for half solar metalicity.

Table 1 Parameters of AGN jet

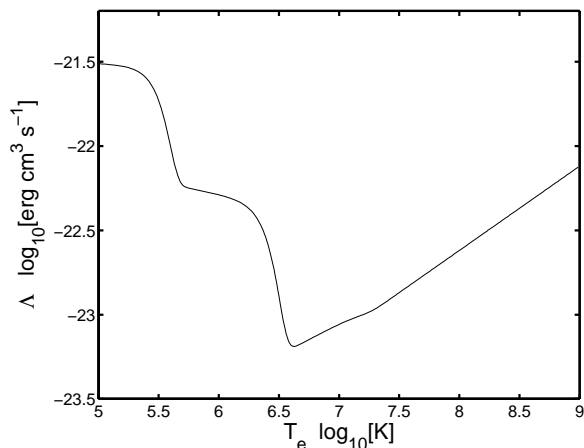| Jet	life span [Myr]	Power [erg/s]
1	25	10^{45}
2	2×25	5×10^{44}

Fig. 1.— Cooling function as function of gas temperature at $\frac{1}{2}z_\odot$.

Fig. 4.— The volume of the bubble as function of the density threshold.

The rate of radiation of energy by a shell of radius r and width dr is:

$$j_{\mathrm{rad}}(r,t) = V_{\mathrm{shell}}(r, r+dr)n_e^2(r,t)\Lambda(T_e(r,t)), \qquad (9)$$

where V_{shell}, n_e and Λ are the shell volume, electron number density and cooling function (Fig. 1), respectively. Under the assumption that the plasma is optically thin, this energy is removed from the computational domain. In the absence of AGN feedback, the system suffers a cooling catastrophe after 3.7×10^8 yr.

Fig. 2 shows n_e and T_e averaged over spherical shells of radius r as functions of r and t. The left panel is for a simulation in which there was only one outburst, while the right column is for a simulation with two outbursts lasting 25 Myr each, and separated by a quiescent period of 25 Myr (Table 1).

The upper row of Fig. 2 shows that the density profile increases to its maximum just before the jet ignites, because radiative losses cause the central plasma to cool, contract and draw plasma in from outlying regions. The jet immediately creates a low-density bubble (blue color near the cluster core). This bubble then moves forward, driven by both jet momentum and buoyancy (Fig 3). The bubble volume is determined by locating cells in which the density is smaller than the averaged density at that radius by a factor f. Fig. 4 shows the resulting volume as a function of f, and on the basis of this plot we set $f = 0.3$.

The temperature profiles in the lower row (Fig. 2) show strong heating during the jet phase, and this heating can be seen to offset the cooling process for about 50 Myr. Results not presented here show that short, powerful jets heat the gas within 10 kpc of the cluster center
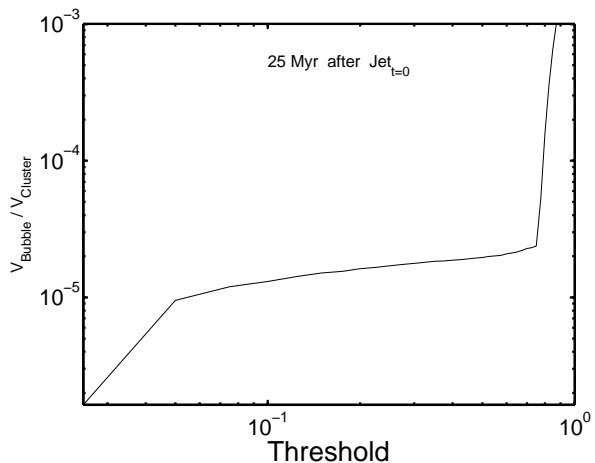
less effectively than a longer-lived lower-power jet, regardless of whether the latter has a single long spell of activity ($\sim 50\,\mathrm{Myr}$) or has two 25-Myr blasts separated by a 25-Myr rest period. The reason is that powerful jets (FR II type) tend to deposit their energy far from the cluster core (Omma et al. 2004). Of the cases presented in Fig. 2, the jet with two cycles couples more efficiently with the gas within the inner cluster region. Although much of the gas uplifted during the first cycle falls back during the 25 Myr jet quiescence, the bulk of the energy injected in the second cycle passes to large radii along the channels that the jet carved through the dense inner ICM during its first cycle (Fig. 3).

4 Conclusion

From the measured bubble volumes and the pressure in the bubbles, we found the energy associated with the bubbles, $U_{\mathrm{bubble}} = pV + \gamma pV/(\gamma - 1)$, where pV is the work done by the jet in creating the bubble and $\gamma pV/(\gamma - 1)$ is the thermal energy within the bubble, and $\gamma = 5/3$ appropriate to a non-relativistic plasma. We found that U_{bubble} is about 6 times less than the energy input from the jet (Binney et al. 2007). Most of the energy not associated with bubbles is divided between the kinetic and potential energy of the gas that is either displaced by the bubbles or entrained in their wake. Some additional energy has been thermalized in the shocks that move ahead of the bubbles. The kinetic and potential energy that surrounds the bubbles will eventually be converted into heat through dissipation of the long-lived gravity waves in which this energy is invested.
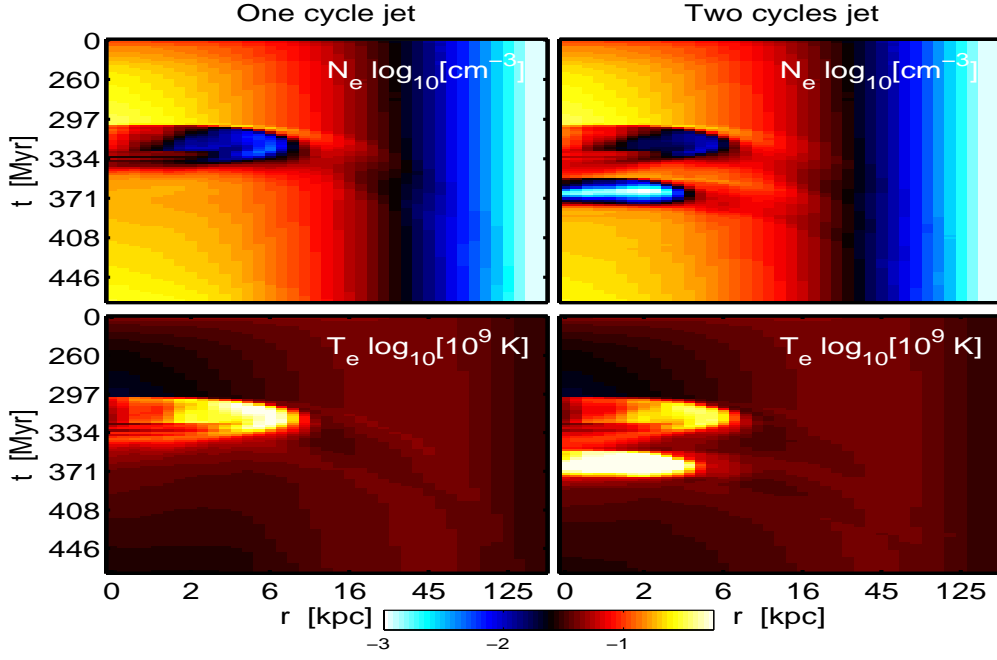
Fig. 2.— Map of radial temperature and density profiles as function of time for one cycle jet (left column) and two cycles jet (right column).
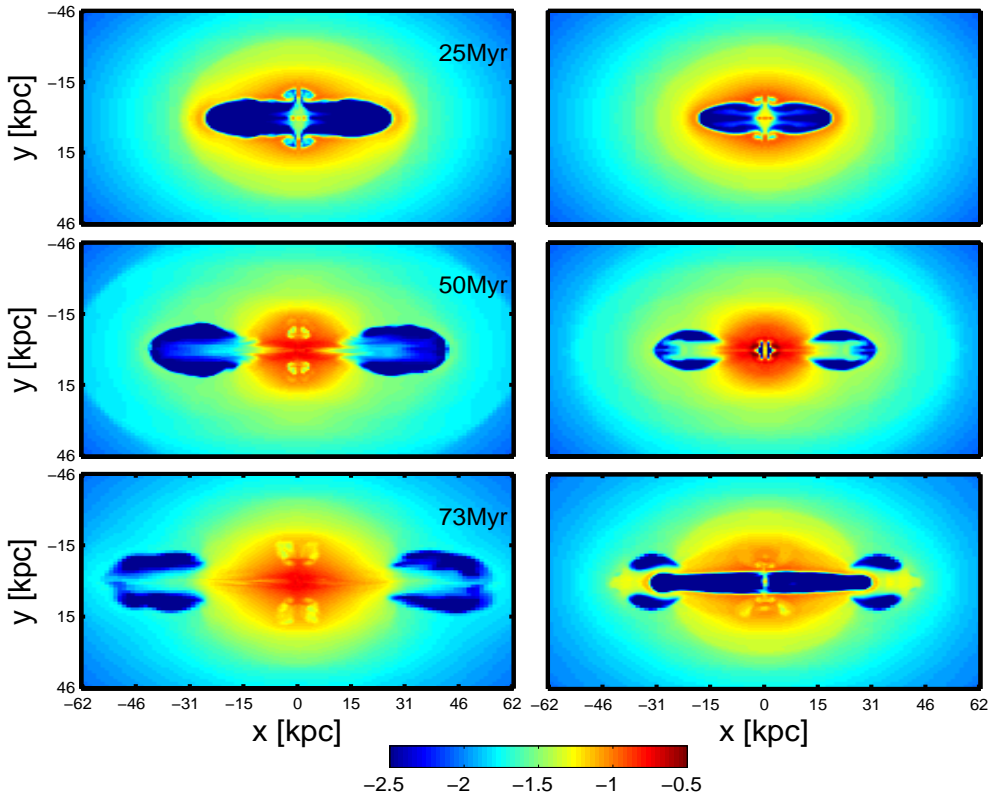

Fig. 3.— Density map along the xy plane (x is the jet axis) and bubble evolution, one cycle jet (left column); two cycles jet (right column). The evolution of the bubble (dark blue region) at different times 25, 50 and 73 Myr after jet ignition.

5 Acknowledgements

References

Basson, J.F. & Alexander, P., 2003, MNRAS, 339, 353

Binney, J., 2005, Phil. Trans. R. S., 363, 739

Binney J., Alouani Bibi F., Omma H., 2007, MNRAS, 377, 142

Binney, J. & Tabor, G., 1995, MNRAS, 276, 663

Birzan L., Rafferty D.A., McNamara B.R., Wise M.W., Nulsen P.E.J., 2004. ApJ, 607, 800

Blandford, R.D., Znajek, R.L., 1977, MNRAS, 179, 433

Brüggen, M. & Kaiser, C.R., 2002, Nat, 418, 301

Bryan G.L., Norman M.L., 1997, in "Computational Astrophysics", ASP Conf. Ser. 123, p.363

Carilli, C.L., Perley, R.A., Harris, D.E., 1994, MNRAS, 270, 173

Cattaneo, A., Teyssier, R., 2007, MNRAS, 376, 1547

Churazov E., Forman W., Jones C., Böhringer H., 2000, A&A, 356, 788

Churazov E., Brüggen M., Kaiser, C.R., Böhringer H., Forman W., 2001, ApJ, 554, 261

David L.P., Nulsen P.E.J., McNamara B.R., Forman W., Jones C., Ponman T. Robertson B., Wise M., 2001, ApJ, 557, 546

Fabian, A.C., Mushotzky, R.F., Nulsen, P.E.J., Peterson J.R., 2001, MNRAS, 321, L20

McNamara, B.R., Wise, M.W., Nulsen, P.E.J., David, L.P., Sarazin, C.L., Bautz, M., Vikhlinin, A., Forman, W.R., Jones, C., Harris, D.E., 2000, ApJL, 534, L135

Navarro, J.F., Frenk, C.S., White, S.D.M., 1995, MNRAS, 275, 720

Nipoti, C., Blundell, K.M & Binney, J.J., 2005, MNRAS, 361, 633

Omma, H., Binney, J., Bryan, G., Slyz, A., 2004, MNRAS, 348, 1105

Peterson et al., 2003, ApJ, 590, 207

Pizzolato, F. & Soker, N., 2005, ApJ, 632, 821

Sutherland, R.S., Dopita, M.A., 1993, ApJS, 88, 253

Woodward, P., Collela, P., 1984, J.Comp.Phys, 54, 115